Probing the Micromechanical Behavior of Semicrystalline Polypropylene Films by Brillouin Spectroscopy

O. Priadilova†, W. Cheng†, G. Tommaseo†, W. Steffen†, J. S. Gutmann†, and G. Fytas*,†,‡

Max Planck Institute for Polymer Research, P.O. Box 3148, 55128 Mainz, Germany, and Department of Materials Science and Technology, University of Crete and FORTH, P.O. Box 1527, 71110 Heraklion, Greece

Received November 2, 2004; Revised Manuscript Received December 17, 2004

ABSTRACT: Inelastic Brillouin light scattering from semicrystalline polypropylene films reveals the presence of up to four bulk and surface phonons. The coexistence of amorphous and crystalline regions in the micrometer range allows for the propagation of two longitudinal acoustic excitations and one transverse acoustic excitation. The surface Rayleigh wave proceeds with a phase velocity intermediate between the two longitudinal counterparts, indicating surface inhomogeneities. The intensity and the frequency of the observed phonons relate to the fraction of sizable (>0.2 μm) spherulites and provide a nondestructive microrheological characterization of the film. The relation of the acoustic excitations to the surface and bulk morphology of the semicristalline films is supported by the X-ray patterns and AFM images.

I. Introduction

Electromagnetic radiation is scattered inelastically by propagating thermal density fluctuations in condensed matter at equilibrium. Brillouin light scattering (BS) is nowadays a powerful, nondestructive technique that uses tandem Fabry−Perot interferometry to record the phonon spectrum of materials in the gigahertz frequency range with high resolution.[1] The incoming and outgoing photons with wave vectors $\mathbf{k}_i$ and $\mathbf{k}_s$ define the scattering wave vector $\mathbf{q} = \mathbf{k}_i - \mathbf{k}_s$ which for homogeneous media over the length scale $O(q^{-1})$ matches the wave vector $\mathbf{k}$ of the selected acoustic phonon, i.e., $\mathbf{q} = \mathbf{k}$ with a phase velocity c. In this case, the experimental spectrum $I(q,\omega)$ displays one Brillouin doublet at a frequency $\pm cq$ on both sides of the elastic (at $\omega = 0$) central Rayleigh line. For inhomogeneous media, however, with characteristic spacing $d = O(q^{-1})$ additional modes are, in principle, expected due to the interaction of light with phonons, particle vibrations, and the periodic lattice. For example, at a given photon scattering wave vector q, lamellar microstructures can display the so-called "Bragg" phonons fulfilling the condition $\mathbf{q} = \mathbf{k} + \mathbf{G}$, where $\mathbf{G}$ is the reciprocal lattice vector G ($=2\pi/d$).[2] Hence, the phonon dispersion $\omega(q)$ can be a sensitive index of the microphase morphology and the grain orientation in ordered diblock copolymer systems.[3]

Thin films, homogeneous over the length scale $O(q^{-1})$, have extensively been studied by BS mainly for the determination of the elastic stiffness coefficients; see, for example, refs 4−7 for hard (metal, semiconductor) films and refs 8−12 for soft (polymer) films. In the field of nanotechnology patterned surfaces are often used in the fabrication of various devices. In few such nanostructured surfaces with a periodic submicrometer grating have the elastic excitations been studied by BS so far.[13−16] For Si surfaces patterned with shallow gratings, the dispersion plot $\omega(q_{||})$ reveals a small gap at the first surface Brillouin zone (π/d) and a hybridization between the surface acoustic modes when the scattering wave vector $q_{||}$ parallel to the surface is perpendicular to the grating grooves.[14] Besides these transverse and longitudinal surface modes, supported polystyrene films with deep gratings allow for the propagation of additional modes of unknown origin.[15] Very recently, the spatial confinement in thin poly(methyl methacrylate)/Si_3N_4 double-layer membranes with distinctly different elastic constants resulted in thickness-dependent longitudinal and transverse standing wave resonances.[16]

Ordered structures are present in simple commodity homopolymers amenable to crystallization, e.g., polypropylene. For spherulites exceeding the probing phonon wavelength, BS should resolve the elastic properties of both crystalline and amorphous regions. In the case of films, the contribution of the surface phonons to the spectrum might provide additional information about the surface rigidity. The use of films rather than bulk samples is compulsory in the case of strong multiple light scattering, and for thickness much larger than the probing wavelength ($\sim q^{-1}$), confinement effects[15,16] are negligible.

In this paper, we report the first, to our knowledge, application of BS to reveal the effect of sizable spherulites on the high-frequency mechanical properties of semicrystalline polymer (isotactic polypropylene (PP)) films. Depending on the thermal treatment, the BS spectrum of PP consists of up to four acoustic excitations. The dispersion $\omega(q_{||})$ and $\omega(q)$ relations of the phonon frequencies and the intensity and the lifetime of the observed modes help identify their origin, yield the film elastic constants, and establish their relation to the film morphology. It is the size of the spherulites rather than the crystallinity that affects the bulk modulus. Hence, BS provides complementary information to established X-ray scattering and calorimetric techniques.

The paper is organized as follows: After the presentation of the experimental methods in the next section,

† Max Planck Institute for Polymer Research.
‡ University of Crete and FORTH.

10.1021/ma047747k CCC: $30.25
Published on Web 02/08/2005

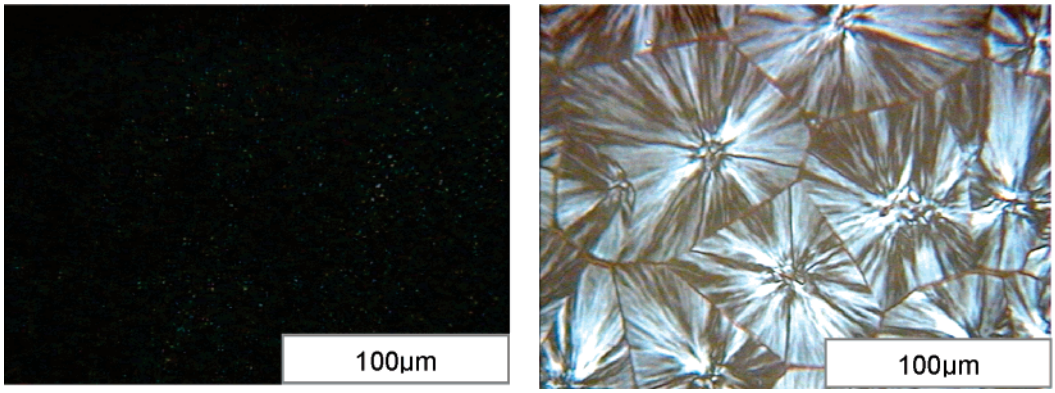

Figure 1. Polarized optical micrographs of the quenched (from 200 to 20 °C) q-PP (a) and the annealed (from 200 to 20 °C at 8 °C/min) a-PP (b) films used in the Brillouin scattering experiments.

we first present the results on quenched PP in section III.A and then discuss the richer phonon spectrum of annealed PP in section III.B. Concluding remarks and perspectives are briefly presented in the last section.

II. Experimental Section

Samples. The material was a commercial isotactic PP with weight-average molecular mass M_w = 400 kDa, number-average molecular mass M_n = 50 kDa, melting point 164 °C, and density ρ = 0.9 g/cm^3. For the preparation of the films used in this experiment with thickness 50−100 μm, PP pellets were melted for 10 min at 200 °C in a press consisting of two heated plates. The films were then either quenched (q-PP) in water at room temperature or slowly cooled (a-PP) in the press at 8 °C/min. Using a Zeiss optical microscope (D-7082) equipped with a color (Hitachi KOD50) camera, the recorded optical micrographs of Figure 1 clearly reveal different crystalline morphology in these two films. Large spherulites are present only in the a-PP film.

X-ray Diffractometry. The degree of crystallinity and the lamellar thickness were estimated by wide-angle (WAXS) and small-angle (SAXS) X-ray scattering experiments, respectively. For the WAXS measurements, a Siemens $\theta-\theta$ diffractometer (D500T) was employed in the reflection geometry. In the SAXS experiment, a 0.8 kW rotating anode X-ray source (Rigaku, RA.Micromax 007) at a wavelength 0.154 nm was used to obtain the scattering intensity profile for angles between 0.1° and 1.1° in steps of 0.02° with a 1.8 m sample to detector distance. The duration of a SAXS measurement was about 1 h.

Brillouin Scattering. Inelastic light scattering spectra $I(\omega)$ were recorded as a function of both the scattering wave vector q (=$(4\pi n/\lambda)$ sin$(\theta/2)$, with n being the refractive index, θ the scattering angle, and λ = 532 nm the laser wavelength) and the component $q_{||}$ parallel to the film surface at a fixed θ = 150° by a six-pass Fabry−Perot interferometer using the setup described elsewhere.[17] The variation of the component of q parallel to the film surface ($q_{||}$) proceeds through the rotation of the film about the optical axis of the goniometer, i.e., changing the angle of incidence θ_r.[12] The polarization of the incident laser beam was perpendicular to the plane of incidence, whereas the polarization of the scattered light was chosen by means of a high-extinction Glan-Thompson analyzer. The laser intensity was relatively low (about 50 mW) and mildly focused using a 30 cm lens. Hence, on the basis of the intensity of the transmitted laser, heating of the films during the record of the BS spectra is excluded.

III. Results and Discussion

A. Quenched PP Film. Figure 2 shows experimental $I(\omega)$ spectra for the **q-PP** film at q = 0.034 nm^1 (θ = 150°) at two different values for the in-plane scattering wave vector component $q_{||}$ (for θ_r = 40° and 50°) at 20 °C. At first glance, the spectra display two Brillouin

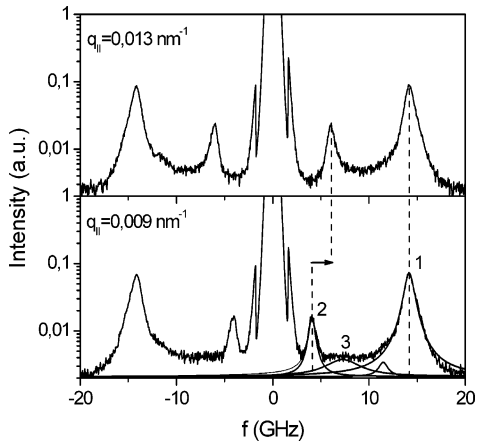

Figure 2. Polarized Brillouin spectra of the free-standing q-PP film at q = 0.034 nm^{-1} and for two values of the photon wave vector $q_{||}$ parallel to the surface as indicated in the plot. Peak 1 relates to the longitudinal bulk phonon, whereas peak 2 is due to the surface mode since its frequency varies with $q_{||}$. The vertical dashed lines denote the frequencies of the two modes. The weak shoulder at the low-frequency side of peak 1 is due to interferometer ghost lines. The solid line denotes the fit of four Lorentzian spectral line shapes to the experimental spectrum.

doublets from which only one (denoted by 2) shifts with $q_{||}$ as indicated by the dashed vertical lines and the arrow in Figure 2. The relation of the peak position of the two modes to the magnitude of $q_{||}$ distinguishes bulk (1) from surface (2) excitations. For a quantitative analysis, the experimental $I(\omega)$ values were represented by a sum of three Lorentzian line shapes using the amplitudes (I_i), the peak positions (ω_i), and the half-width at half-height (Γ_i) as free parameters (i = 1−3). The third Lorentzian is necessary to describe the frequency region between modes 1 and 2, while the small shoulder at the low-frequency wing of mode 1 arises from the ghost contribution, i.e., the interferometer higher order. The solid line in the lower panel of Figure 2 is then the representation of the experimental spectrum considering the four contributions. Next, we consider the two main peaks and postpone the discussion of intermediate spectral feature 3 to section B.

The amplitude I_i and line width Γ_i of modes 1 and 2 (Figure 2) are expected to display different $q_{||}$ dependencies. The intensity $I_1 \approx k_B T \beta_s$ is q-independent due to local adiabatic density fluctuations controlled by the value of the compressibility β_s, and in the hydrodynamic limit,[18] the line width Γ_1 is q^2-dependent. In fact, Figure 3 demonstrates the insensitivity of these two quantities

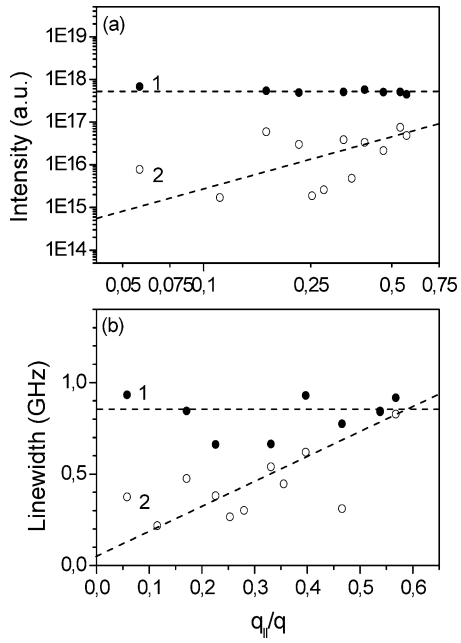

Figure 3. Inelastic scattering amplitude (a) and line width (b) for the surface (2) (open circles) and bulk (1) (solid circles) modes of Figure 2 plotted as a function of $q_{||}$ in a log−log plot. The dashed lines are to guide the eye.

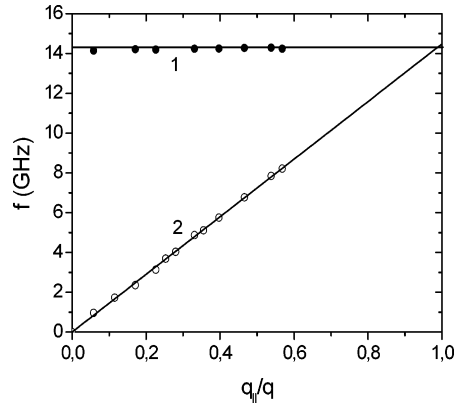

Figure 4. Dispersion relation $f\,(=\omega/2\pi)$ versus $q_{||}/q$ at constant q (=0.034 nm^{-1}) in the q-PP film obtained from the spectra of Figure 2. Solid and open circles indicate the longitudinal phonon (1) in the bulk of q-PP and the surface mode (2), which reveals longitudinal polarization as well; the frequencies of the two modes coincide at $q_{||}/q = 1$.

to $q_{||}$ variation at constant q for the bulk phonon (1). On the contrary, both I_2 and Γ_2 also with longitudinal polarization[12] (see Figure 4 below) clearly increase with $q_{||}$, underlining the surface character of this phonon. Within experimental error, Figure 3 suggests the scalings $I_2 \approx q_{||}$ and $\Gamma_2 \approx q_{||}$; i.e., long wavelength surface ripples are less probable but long-lived. Like for the bulk phonons, the hydrodynamic[19] viscous fluid behavior would predict the stronger $\Gamma_2 \approx q_{||}^2$ dependence. Since longitudinal modes do not ripple the surface, their appearance implies coupling to the shear waves. Hence, the observed $q_{||}$ dependence of I_2 and Γ_2 might relate to the chain elasticity.

The central result in the wave propagation is the dispersion relation of the phonon frequencies $f_i\,(=\omega_i/2\pi)$ obtained from the experimental $I(\omega)$ as a function of q and $q_{||}$. On the basis of the latter dispersion shown in Figure 4 at a given q, there is one longitudinal acoustic phonon (solid circles) propagating in the bulk of the film

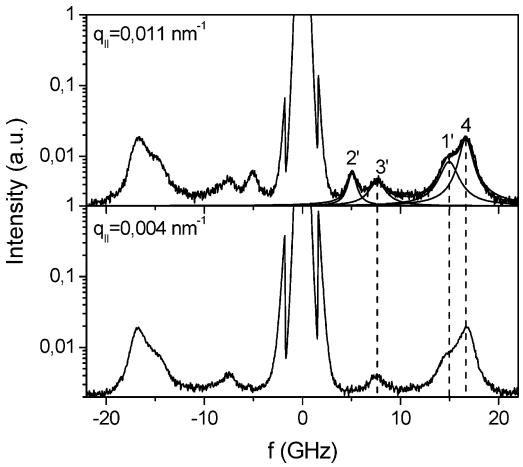

Figure 5. Polarized Brillouin spectra at $q = 0.034$ nm^{-1} and at two different values of $q_{||}$ for the free-standing polypropylene film obtained by slowly (8 °C/min) annealing (a-PP) from the molten state to ambient temperature. The a-PP film shows two additional elastic excitations denoted as 3′ and 4 independent of $q_{||}$ at constant q. The peaks designated by 1′ and 2′ correspond to peaks 1 and 2 of Figure 2 albeit somewhat shifted to higher frequencies. The solid line denotes the fit of four Lorentzian spectral line shapes to the experimental spectrum.

with $\omega_1 = c_L q$ (see Figure 6b below) and one surface -guided primarily longitudinal phonon with $\omega_2 = cq_{||}$. The phase velocity $c_L = 2590$m/s leads to the modulus $M\,(=\rho c_L^2) \approx 6$ GPa (also known as the elastic stiffness constant c_{11}), which is in a good agreement with reported values for PP.[20] Like for polycarbonate films,[12] the observed surface waves are very close to the longitudinal (c_L) and not to the transverse (c_t) bulk value. Theoretically,[21] the velocity of the usual Rayleigh surface excitation is $0.933c_t$, i.e., localized almost in the transverse bulk threshold for an isotropic solid with Poisson ratio 1/3. Calculations on the relative strength of these matter displacements at soft surfaces are missing. The observation of the longitudinal surface mode is rather unexpected since this mode is polarized parallel to the surface and hence does not ripple it. It was suggested[14b] that corrugated metal surfaces could rotate the polarization of the longitudinal mode so that it can ripple the surface.

The presence of a single bulk phonon suggests a homogeneous q-PP film for length scales above about q^{-1} as is clearly confirmed by the optical micrograph in Figure 1a. The absence of sizable spherulites, however, does not imply a fully amorphous film. In fact, X-ray scattering (Figure 8 below) reveals a short-range crystallinity (∼37%) which apparently does not affect the elasticity of the effective medium. To assess the effect of submicrometer heterogeneities on the high-frequency elasticity, we utilize the slowly annealed a-PP film with the documented spherulite crystalline morphology in Figure 1b.

B. Annealed PP Film. The Brillouin spectra of the a-PP film in Figure 5 display up to four acoustic excitations depending on the magnitude of $q_{||}$. The additional peaks in the spectrum of the a-PP film present bulk phonons (1′, 3′, 4) since their frequencies do not depend on $q_{||}$ at constant q. The experimental $I(\omega)$ can be represented by four Lorentzians (solid lines in Figure 5) plus the ghost line as was the case for q-PP in Figure 2. The frequencies f_i (i = 1−4) of the four phonons in a-PP are shown in the dispersion plot of

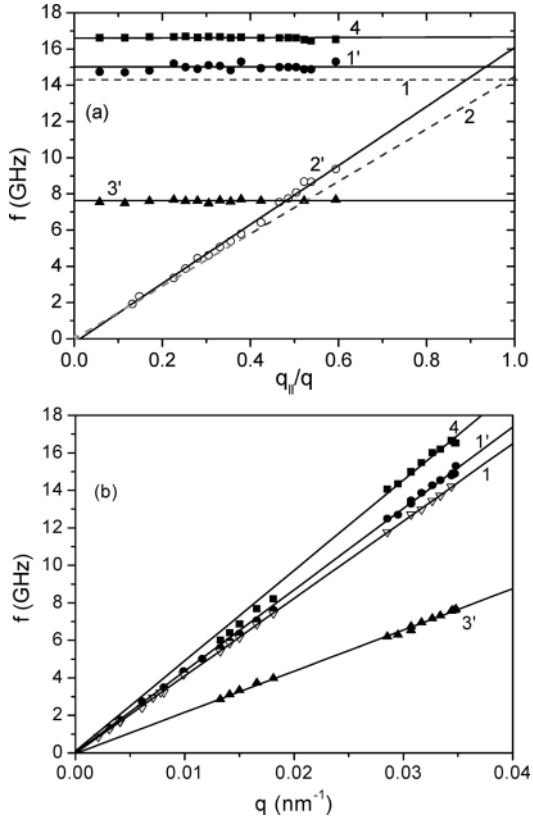

Figure 6. Dispersion relation $f\,(=\omega/2\pi)$ versus $q_{||}/q$ at constant q (=0.034 nm^{-1}) (a) and versus q (b) obtained from the experimental Brillouin spectra of the a-PP film. The dispersion relations in q-PP (Figure 4) are denoted by the two dashed lines (modes 1 and 2 in Figure 4). Solid symbols indicate the two longitudinal phonons (1′, 4) and the transverse phonon (3′) in the bulk of the a-PP film, whereas the open circles denote the surface mode (2′), which reveals longitudinal polarization; the frequency of the surface mode at $q_{||}/q = 1$ assumes an intermediate value between those of the bulk longitudinal phonons.

Figure 6a along with the two frequencies of modes 1 and 2 of Figure 4 indicated by dashed lines for the sake of clarity.

According to the displayed relations, the a-PP film displays three bulk phonons and one surface phonon. The former acoustic excitations present two longitudinal polarizations due to the closeness to the bulk acoustic phonon (1) in the q-PP film and one transverse phonon (3′).The bulk origin of these phonons is verified by their dependence on the magnitude of q shown in Figure 6b. Note that the frequencies of the bulk phonon (1) and the surface phonon (2) excitation in q-PP are systematically lower than those of the respective excitations (1′ and 2′) in a-PP (Figure 6). The slope of the linear dispersion $f \approx q$ yields the values $c_L = 2590$ m/s for the longitudinal sound velocity in q-PP and $c_L' = 2730$ m/s, $c_2 = 3026$ m/s, and $c_T = 1380$ m/s for the two longitudinal velocities and shear sound velocity in a-PP; a typical error in the evaluation of the longitudinal sound velocities is about 2%. The intensity of the transverse phonon (mode 3 in Figure 2) is much stronger in the a-PP film (mode 3′ in Figure 5) due to the presence of solid spherulites (Figure 1b). Note that only the elastic constant c_{44} $(=\rho c_T^2)$ is accessible due to the random orientation of the spherulites.

The two longitudinal phonons in a-PP relate to the heterogeneous morphology of the film over length scales larger than the phonon wavelength Λ $(=2\pi/q)$ with

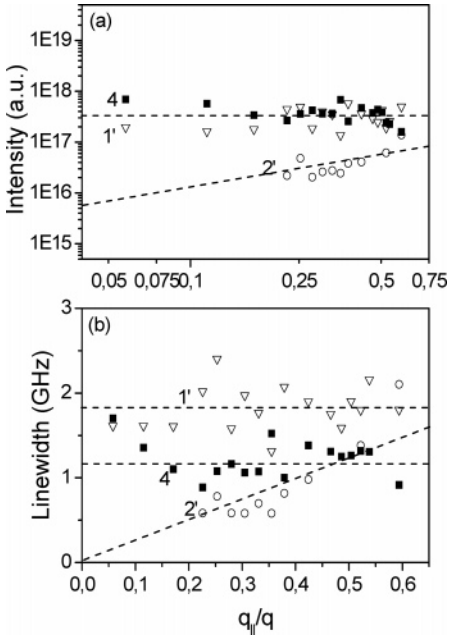

Figure 7. Inelastic scattering amplitude (a) and line width (b) for the surface (2′) (open circles) and bulk (1′, solid circles; 4, solid squares) modes in the a-PP film plotted as a function of $q_{||}$. (a) is a log−log plot. The dashed lines are to guide the eye.

values in the range 0.18−2 μm. In addition, the sufficient elastic constant contrast $(c_2/(c_L')^2)$ between amorphous and crystalline PP allows the detection of modes 1′ and 4. Hence, the highest frequency phonon (4) (Figures 5 and 6) is attributed to the sound propagation within the crystalline microphases. The semicrystalline a-PP is then envisaged as an effective medium with c_L' falling between c_L and c_2 of the amorphous and crystalline pure phases, respectively. Since the compressibility β_s $(=1/\rho(c_L')^2)$ of the effective medium is a composition average of the compressibilities[22] of the individual phases, the experimental c_L' can be captured by a crystalline fraction of about 35%.

The physical state of a-PP appears to affect the intensity and the lifetime of the bulk phonon (1′ and 4) as shown in Figure 7. While these quantities exhibit the anticipated (Figure 3) insensitivity to the $q_{||}$ variation, the phonon at peak 1′ decays much faster than that at peak 1 in q-PP probably due to significant phonon scattering by the solid spherulites in the a-PP film. The lifetime of the phonon at peak 4 in the crystalline regions, albeit longer than for that at peak 1′, is still short for solids, reflecting phonon scattering due to imperfections. The relative intensities of these two phonons in Figure 7a, $I(1')/I(4) \approx 0.8$, should depend on the component compressibilities and the fraction α' of the spherulites (Figure 1b). Assuming similar densities, $I(1')$ should be about 20% higher than $I(4)$ because of the compressibility ratio, i.e., $(c_2/c_L)^2$. Hence, the experimental intensity ratio might be approximated by $((1-\alpha')/\alpha')(c_2/c_L)^2$, which leads to $\alpha' \approx 0.6$. This value is, however, 2 times larger than the estimated fraction from the sound velocity data (Figure 6b), but similar to the computed crystallinity (∼0.6) from the WAXS data below. Small spherulites not captured by the Brillouin shift, contribute, however, to the intensity $I(4)$ since Brillouin scattering arises from local density fluctuations. Nevertheless, the simple relation between Bril-

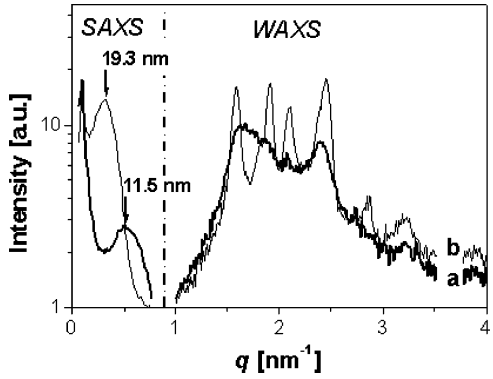

Figure 8. SAXS and WAXS profiles for the q-PP (thick line) and a-PP (thin line) films. The arrows indicate the SAXS peaks due to the lamella long spacings of 11.5 and 19.3 nm in the q-PP and a-PP films, respectively.

louin intensities and α′ is approximate even though it correctly captures the trend.

X-ray scattering is an established experimental technique for the study of semicrystalline polymers. Figure 8 shows SAXS and WAXS intensity distributions for the same q-PP and a-PP films used in the Brillouin experiment. The a-PP film possesses a well-developed crystalline phase as is evident from the WAXS reflections and the strong SAXS peak, yielding a long period distance $D = 19.3$ nm. In comparison, the profiles for q-PP exhibit much weaker crystalline features. The results were used to estimate the average lamella thickness $L_c = \alpha D$. The degree of crystallinity α is given by the fraction $(\int q^2 I_{cr}\, dq)/(\int q^2 I\, dq)$ of the total $I(q)$ WAXS scattering due to the crystalline $I_{cr}(q)$ contribution.[23] The values of these morphological parameters are listed in Table 1. The lamella thickness is approximately 3 times greater than in the q-PP film, confirming the effect of the thermal treatment on the morphology of the two films. The determined degree of crystallinity was estimated to be 60% and 37% for a-PP and q-PP, respectively.

These reliable estimates along with the optical micrographs and the Brillouin spectra (Figures 2 and 5) suggest that the two films are mainly distinguished by the size of the spherulites. The crystallites in q-PP are too small to affect the propagation of phonons with

Table 1. Morphological Characteristics of the Polypropylene Films

sample	degree of crystallinity α (%)	long period D (nm)	lamella thickness L_c	elastic constants c_{11}, c_{44} (GPa)
a-PP	∼60	19.3	11.6	8.2,1.7
q-PP	∼37	11.3	4.3	6.0

submicrometer wavelengths. Brillouin spectroscopy can therefore discriminate the size of spherulites indiscernible by X-ray scattering and moreover assess the micromechanics of semicrystalline films.

The propagation of the surface phonons (2 and 2′) in the two free-standing films shows some distinct features. Both have longitudinal polarizations (Figure 6a), but mode 2′, in contrast to mode 2, does not propagate with the phase velocity c_L' of the effective a-PP medium. Instead, it adopts a speed between c_L' and c_2, the speed of sound in the two microphases. This intriguing finding might suggest surface modification, e.g., a higher density and hence crystallinity than in the bulk, and could open a new application of this optical technique. In fact, the height AFM images of Figure 9 complement the optical images of Figure 1. Both techniques indicate large spherulites of approximately 80 μm in the a-PP film located at the surface and in the bulk. The topographic image of the a-PP film (Figure 9, right panel) shows the central part of nucleation of a spherulite with different sectors. On the contrary, the AFM image of q-PP (Figure 9, left panel) does not reveal a well-defined spherulite morphology. Instead, the sample appears to consist entirely of about 2 μm granules, implying inhibition of spherulite structures. The micrographs show bright and dark regions which relate to harder and softer areas, respectively, indicative of surface microsegregation. To investigate the manifestation of surface morphology on the Brillouin spectrum, a controlled deposition of crystalline layers with various thicknesses is needed for a quantitative assessment of the penetration depth (∼Λ) of the surface excitations.

IV. Concluding Remarks

Inelastic (Brillouin) light scattering from semicrystalline homopolymers can measure the high-frequency elastic constant (c_{11}) of the two microphases if the

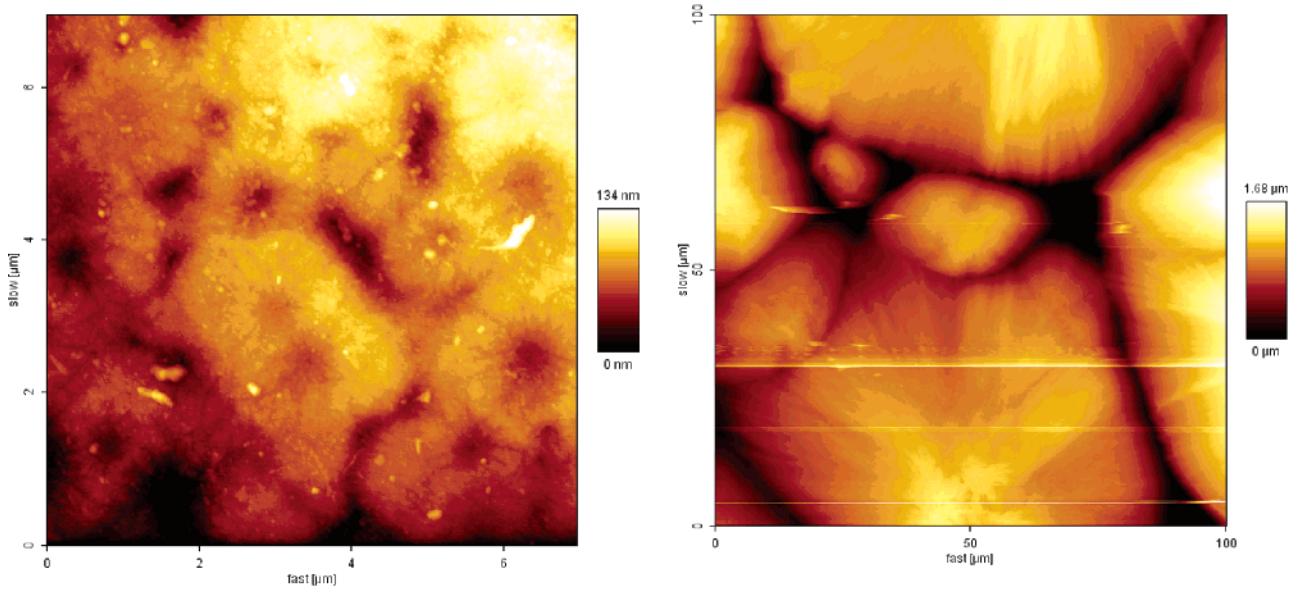

Figure 9. Height images of q-PP (left panel) and a-PP (right panel).

formed spherulites exceed the size of the wavelength of the probed phonons. In this case, the film is inhomogeneous over the relevant length scales, and there is an access to the transverse phonon in the crystalline phase, yielding the elastic constant c_{44} as well.

The degree of crystallinity estimated from c_{11} of the effective medium is expectedly lower than the value from WAXS given the size requirement for revealing crystallinity by the Brillouin scattering. On the other hand, a simple account of the Brillouin line intensities associated with the longitudinal phonon propagating in the two phases leads to a much higher crystallinity value which is close to the WAXS value.

Despite the significant thickness of the used films, there is still a contribution from surface inelastic scattering, revealing a surface phonon with longitudinal polarization. In the quenched polypropylene film, this surface phonon propagates with the phase velocity c_L of the longitudinal phonon in the bulk material. In the annealed film with large spherulites, the phase velocity of the surface mode falls between the longitudinal sound velocities in the bulk amorphous and crystalline phases. This finding suggests surface microsegregation supported by AFM images.

References and Notes

(1) Kriegs, H.; Steffen, W.; Fytas, G.; Monaco, G.; Dreyfus, K.; Fragouli, M.; Pitsikalis, M.; Hadjichristidis, N. *J. Chem. Phys.* **2004**, *121*, 2376.

(2) Urbas, A.; Thomas, E. L.; Kriegs, H.; Fytas, G.; Penciu, R. S.; Economou, E. N. *Phys. Rev. Lett.* **2003**, *90*, 108302.

(3) Tommaseo, G.; Penciu, R. S.; Fytas, G.; Economou, E. N.; Hashimoto, T.; Hadjichristidis, N. *Macromolecules* **2004**, *37*, 5006.

(4) Sandercock, J. R. *Phys. Rev. Lett.* **1973**, *29*, 2600.

(5) Bortolani, V.; Nizzoli, F.; Santoro, G.; Malvin, A.; Sandercock, J. R. *Phys. Rev. Lett.* **1979**, *43*, 224.

(6) Grimsditch, M.; Bhadra, R.; Schuller, I. K. *Phys. Rev. Lett.* **1987**, *58*, 1216.

(7) Hillebrands, B.; Lee, S.; Stegeman, G. I.; Cheng, H.; Potts, J. E.; Nizzolli, F. *Phys. Rev. Lett.* **1988**, *60*, 832.

(8) Nizzoli, F.; Hillebrands, B.; Lee, S.; Stegemann, G. I.; Duda, G.; Wegner, G.; Knoll, W. *Phys. Rev.* **1989**, *40*, 3323.

(9) Sun, L.; Dutcher, J. R.; Giovannini, L.; Nizzoli, F.; Stevens, J. R.; Ord, J. L. *Appl. Phys.* **1994**, *75*, 7482.

(10) Forrest, J. A.; Rowat, A. C.; Dalnocki-Veres, K.; Stevens, J. R.; Dutcher, J. R. *J. Polym. Sci., Part B: Polym. Phys.* **1996**, *34*, 3009.

(11) Hotz, R.; Krueger, J. K.; Possart, W.; Tadros-Morgane, R. *J. Phys.: Condens. Matter* **2001**, *13*, 7953.

(12) Tommaseo, G.; Lescanne, M.; Steffen, W.; Fytas, G.; Stamm, M. *J. Polym. Sci., Part B: Polym. Phys.* **2004**, *42*, 3311.

(13) Roberston, W. M.; Grimsditch, M.; Moretti, A. L.; Kaufman, R. G.; Hulse, G. R.; Fullerton, E.; Schuller, I. K. *Phys. Rev. B* **1990**, *41*, 4986.

(14) Dutcher, J. R.; Lee, S.; Hillebrands, B.; McLaughlin, G. J.; Nickel, B. G.; Stegeman, G. I. *Phys. Rev. Lett.* **1992**, *68*, 2464. Giovannini, L.; Nizzoli, F.; Malvin, A. M. *Phys. Rev. Lett.* **1992**, *69*, 1572.

(15) Hartschuh, R.; Ding, Y.; Roh, J. H.; Kisliuk, A.; Sokolov, A. P.; Soles, C. L.; Jones, R. L.; Hu, T. J.; Wu, W. L.; Mahorowala, A. P. *J. Polym. Sci., Part B: Polym. Phys.* **2004**, *42*, 1106.

(16) Bandhu, R. S.; Zhang, X.; Sooryakumar, R.; Bussmann, K. *Phys. Rev. B* **2004**, *70*, 075409.

(17) Penciu, R. S.; Kriegs, H.; Petekidis, G.; Fytas, G.; Economou, E. N. *J. Chem. Phys.* **2003**, *37*, 5224.

(18) Berne, B.; Pecora, R. *Dynamic Light Scattering*; Wiley: New York, 1976.

(19) Harden, J. L.; Pleiner, H.; Pincus, P. A. *J. Chem. Phys.* **1991**, *94*, 5208.

(20) Kumar, S. R.; Renusch, D. P.; Grimsditch, M. *Macromolecules* **2000**, *33*, 1819. Cavanaugh, D.; Wang, C. H. *J. Appl. Phys.* **1982**, *53*, 2793.

(21) Landau, L. D.; Lifshitz, E. M. *Theory of Elasticity*; Pergamon: Oxford, 1970.

(22) Sheng, P. *Introduction to wave scattering. Localization and Mesoscopic Phenomena*; Academic Press: San Diego, 1995.

(23) Roe, R. J. *Methods of X-ray and Neutron Scattering in Polymer Science*; New York, Oxford, 2000.

MA047747K